

RSC Advances



This is an *Accepted Manuscript*, which has been through the Royal Society of Chemistry peer review process and has been accepted for publication.

Accepted Manuscripts are published online shortly after acceptance, before technical editing, formatting and proof reading. Using this free service, authors can make their results available to the community, in citable form, before we publish the edited article. This *Accepted Manuscript* will be replaced by the edited, formatted and paginated article as soon as this is available.

You can find more information about *Accepted Manuscripts* in the [Information for Authors](#).

Please note that technical editing may introduce minor changes to the text and/or graphics, which may alter content. The journal's standard [Terms & Conditions](#) and the [Ethical guidelines](#) still apply. In no event shall the Royal Society of Chemistry be held responsible for any errors or omissions in this *Accepted Manuscript* or any consequences arising from the use of any information it contains.

Cite this: DOI: 10.1039/c0xx00000x

www.rsc.org/xxxxxx

ARTICLE TYPE

Noble-metal-free Cu₂S-modified photocatalysts for enhanced photocatalytic hydrogen production by forming nanoscale p-n junction structure

Yubin Chen*, Zhixiao Qin, Xixi Wang, Xu Guo and Liejin Guo*

Received (in XXX, XXX) Xth XXXXXXXXX 20XX, Accepted Xth XXXXXXXXX 20XX
DOI: 10.1039/b000000x

Developing efficient noble-metal-free photocatalysts was of great meaning for the large-scale application of photocatalytic hydrogen production. Herein, low-cost and environment-friendly p-type Cu₂S was successfully loaded on n-type CdS photocatalyst by an in-situ method to achieve efficient Cu₂S/CdS hybrid photocatalysts. Cu₂S nanoparticles of ca. 50 nm were intimately assembled on the surface of polyhedral CdS nanocrystals, giving rise to the formation of numerous nanoscale p-n junctions between p-type Cu₂S and n-type CdS. Compared to single CdS, Cu₂S/CdS exhibited apparently increased photocatalytic hydrogen production under visible light irradiation. The generated nanoscale p-n junctions in Cu₂S/CdS, leading to the enhanced charge separation efficiency and better utilization of visible light, were crucial to the improved photocatalytic activity. During the photocatalytic reaction, Cu₂S nanoparticles captured the photogenerated holes in CdS and served as the active sites for the surface oxidation reaction. The photocatalytic property of Cu₂S/CdS photocatalysts was influenced by the Cu/Cd molar ratio, with the optimal one of 0.05. P-type Cu₂S could also be utilized for improving the photocatalytic activities of n-type ZnIn₂S₄ and n-type TiO₂ by forming efficient p-n junctions, indicating the general applicability of p-type Cu₂S. This work demonstrates that forming p-n junction structure was a useful strategy for developing efficient noble-metal-free hybrid photocatalysts.

1. Introduction

Photocatalytic hydrogen production from water using solar energy has been considered as a promising route to solve the increasing energy and environmental problems.¹⁻³ The key issue for its industrial application is to develop photocatalysts necessitating high efficiency, long-term stability, and low cost. However, most of semiconductor photocatalysts owns poor activity due to rapid charge recombination and insufficient surface reactive sites. Cocatalysts, which can effectively capture the photogenerated electrons/holes to enhance the charge separation efficiency, provide active sites for surface redox reaction, and decrease the surface reaction overpotential, are believed to be essential to achieving highly efficient photocatalytic hydrogen production.⁴

The most common and effective cocatalyst is Pt, which is widely applied for various photocatalysts. Other noble metals, such as Ru, Rh, Au and Pd, are also effective cocatalysts owing to the similar physicochemical properties like Pt.^{5,6} Nonetheless, the high price and low reserve of noble metals limit the large-scale application. Therefore, seeking efficient noble-metal-free photocatalysts is of critical importance. Recently, it has been demonstrated that a series of transition metal sulfides could promote the photocatalytic hydrogen production instead of Pt. Li's group reported that loading MoS₂ or WS₂ on CdS photocatalysts could give rise to efficient charge separation by

forming intimate heterojunctions to achieve high activities.^{7,8} Xu's group revealed that NiS could act as efficient cocatalyst to significantly improve the hydrogen production of CdS photocatalysts. The apparent quantum efficiency of NiS/CdS at 420 nm reached 51.3%.⁹ Xie's group discovered that CuS could accelerate the photogenerated charge separation of CdS photocatalysts and subsequently the photocatalytic hydrogen production.¹⁰ Besides of CdS, the photocatalytic properties of various semiconductor photocatalysts such as Cd_xZn_{1-x}S, CuGa₃S₅, TiO₂, ZnO and C₃N₄ could also be enhanced by the deposition of such metal sulfides, indicating their general applicability.¹¹⁻¹⁵ However, up to now, highly efficient transition-metal sulfide promoters with low price and earth-abundant elements are still limited. Meanwhile, the reported action mechanisms of such metal sulfides are quite different. As a consequence, it is necessary to study the general coupling principle between photocatalysts and such transition-metal sulfides and as a guidance to develop efficient noble-metal-free hybrid photocatalysts.

The basic requirement of coupling different semiconductors to enhance the photocatalytic activity is to form efficient heterojunction structure between different components, which is crucial to the improvement of charge separation efficiency. For example, as noble metal is deposited on semiconductor photocatalysts, the Schottky junction is generated between the

noble metal and the semiconductor photocatalyst, which can lead to the efficient charge separation.⁴ Coupling semiconductors with different band structures to generate heterojunction structure can also result in the efficient charge separation.¹⁶ When p-type semiconductor is combined with n-type semiconductor, p-n junction can be formed between the two semiconductors. Across the p-n junction region, a built-in electric field is achieved, which can efficiently promote the separation of photogenerated electrons/holes.¹⁷ As we know, a number of reported photocatalysts are n-type semiconductors, such as CdS, ZnIn₂S₄ and TiO₂.¹⁸⁻²⁰ Therefore, Coupling suitable p-type semiconductors to promote the photocatalytic properties of n-type semiconductor photocatalysts can be expected. P-type NiO and p-type NiS have been demonstrated to be efficient cocatalysts to promote the photocatalytic activities of n-type semiconductor photocatalysts by forming p-n junctions.^{21,22} However, more efficient p-type semiconductor promoters, especially the ones with wide applicability should be explored.

Cu₂S is a p-type semiconductor with a bulk bandgap of 1.2 eV.²³ Due to its low cost and earth-abundant elements, Cu₂S has been utilized for solar cells, optoelectronic devices and photocatalytic degradation of organic pollutants.²⁴⁻²⁸ However, the utilization of Cu₂S in the area of photocatalytic hydrogen production has been seldom reported.²⁹ Herein, we firstly prepared n-type CdS nanocrystals with polyhedral morphology. Then Cu₂S nanoparticles were deposited by an in-situ method to obtain Cu₂S/CdS photocatalysts. A number of well-dispersed nanoscale p-n junctions were developed in the hybrid photocatalysts, which could efficiently improve the charge separation, leading to the much enhanced photocatalytic activity. P-type Cu₂S was also coupled with n-type TiO₂ and n-type ZnIn₂S₄. Interestingly, the improved activities were also achieved by forming nanoscale p-n junction structure, indicating the good applicability of p-type Cu₂S.

2. Experimental

Cadmium nitrate tetrahydrate (Cd(NO₃)₂·4H₂O), copper nitrate trihydrate (Cu(NO₃)₂·3H₂O), sodium hydroxide (NaOH), sodium sulfide nonahydrate (Na₂S·4H₂O), sodium sulfite (Na₂SO₃), thioacetamide (C₂H₅NS), and ethanol (C₂H₆O) were purchased from Sinopharm Chemical Reagent Co., Ltd. All chemicals were used as purchased without further purification.

2.1 Synthesis of CdS photocatalysts

CdS photocatalysts were synthesized by a hydrothermal method. Briefly, 0.01 mol of Cd(NO₃)₂·4H₂O was firstly added into 50 mL of 1.0 M NaOH aqueous solution. The suspension was stirred uniformly and 0.02 mol of thioacetamide was subsequently added with magnetic stirring. The obtained suspension was then heated for 48 h at 200 °C in a Teflon-lined autoclave. After the autoclave cooled naturally in air, the products were washed with ethanol and deionized water several times and dried in vacuum at 80 °C for 5 h.

2.2 Deposition of Cu_xS onto CdS photocatalysts

Cu_xS was deposited onto CdS photocatalysts by an in-situ method. Before photocatalytic hydrogen production, appropriate amounts of Cu(NO₃)₂ solution were added into the Na₂SO₃/Na₂S reaction

solution containing 0.2 g of CdS powders. The suspension was then stirred for 0.5 h with nitrogen purged to obtain Cu_xS/CdS hybrid photocatalysts for photocatalytic reaction. The achieved products were denoted as Cu_xS/CdS-n, where n represented the Cu/Cd molar ratio. Pure Cu_xS was also synthesized for analysis. Typically, 0.005 mol of Cu(NO₃)₂·3H₂O was added into 190 mL of 0.25 M Na₂SO₃/0.35 M Na₂S aqueous solution, and stirred for 0.5 h with nitrogen purged. The obtained products were collected, washed with deionized water, and dried in vacuum at 80 °C for 5 h.

2.3 Characterization

The X-ray powder diffraction (XRD) pattern was examined by a PANalytical X'pert MPD Pro X-ray diffractometer (Cu K α radiation). UV-visible (UV-vis) absorption spectrum was recorded using a HITACHI U-4100 spectrophotometer. The morphology of the photocatalysts was characterized with a JEOL JSM-7800F field-emission scanning electron microscope (FESEM), to which an Oxford energy dispersive X-ray spectroscopy (EDX) system X-max50 was coupled for EDX-SEM mapping analysis. The close examination of the morphology was carried out on a JEOL 1200CX transmission electron microscope (TEM). The X-ray photoelectron spectroscopy (XPS) measurement was conducted on a Axis Ultra, Kratos (UK) multifunctional X-ray photoelectron spectrometer (Al K α radiation). Binding energies were calibrated relative to the C 1s peak (284.8 eV) from adventitious carbon adsorbed on the surface of the samples. The photoluminescence (PL) property was analyzed at room temperature on a PTI QM-4 fluorescence spectrophotometer.

2.4 Photocatalytic hydrogen production

Photocatalytic hydrogen production was tested with stirring under visible light irradiation in a side irradiation Pyrex cell with a water jacket (Fig. S1). The efficient irradiation area of the cell was 15.90 cm². 0.2 g of photocatalysts were added into 190 mL of aqueous solution containing 0.25 M Na₂SO₃/0.35 M Na₂S as sacrificial reagents, and appropriate amount of Cu_xS was deposited by the above mentioned in-situ method. Nitrogen was purged through the cell before reaction to remove oxygen. A 300 W Xe lamp equipped with a cutoff filter ($\lambda \geq 420$ nm) was used as the light source, and the temperature was kept at 35 \pm 0.2 °C for all photocatalytic reactions by flowing water with controlled temperature of 35 °C through the water jacket. The amount of generated hydrogen was detected by an on-line TCD gas chromatograph (NaX zeolite column, N₂ as carrier gas). The blank experiments in the absence of irradiation or photocatalyst showed no appreciable hydrogen production. The apparent quantum yield (AQY) was calculated by the equation (1). Specifically, in order to test the AQY of the photocatalyst at 420 nm, a 420 nm band-pass filter was coupled with the 300 W Xe lamp as the light source. The amount of generated hydrogen was detected by an on-line TCD gas chromatograph, and the light intensity at 420 nm was measured by a fiber optic spectrometer. The calculation method of the number of incident photons can be found in the supporting information.

$$\begin{aligned} \text{AQY}(\%) &= \frac{\text{The number of reacted electrons}}{\text{The number of incident photons}} \times 100 \quad (1) \\ &= \frac{\text{The number of evolved H}_2 \text{ molecules} \times 2}{\text{The number of incident photons}} \times 100 \end{aligned}$$

3. Results and discussion

3.1 Demonstration of generating Cu₂S and Cu_xS/CdS

Fig. 1 shows the XRD patterns of different samples. The diffraction peaks of hydrothermally synthesized CdS could be well assigned to wurtzite CdS with a typical hexagonal structure (JCPDS No. 06-0314).³⁰ The sharp peaks indicated their good crystallinity. Subsequently, the diffraction peaks of as-synthesized Cu_xS observed at 2θ values of 27.91°, 32.38°, 46.46°, and 54.88° could be indexed to (111), (200), (220) and (311) planes of Cu₂S cubic phase (JCPDS No. 84-1770).^{31,32} For Cu_xS/CdS hybrid photocatalysts, there were only diffraction peaks corresponding to those of wurtzite CdS, possibly owing to the low loading amount and high dispersion of Cu_xS particles. It was noticed that the intensities of CdS diffraction peaks were decreased with the increasing amount of Cu_xS, probably due to the covering of Cu_xS particles onto the surface of CdS.

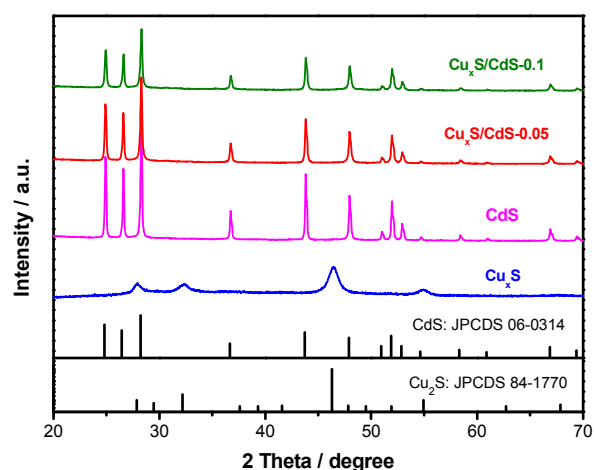


Fig. 1 XRD patterns of CdS, Cu_xS, and Cu_xS/CdS samples with various Cu/Cd molar ratios.

To further analyse the valance states of copper in Cu_xS and Cu_xS/CdS, XPS measurements were carried out. As indicated in Fig. 2a, the Cu 2p XPS spectrum of Cu_xS revealed that the binding energies of Cu 2p_{3/2} and Cu 2p_{1/2} peaks were respectively located at 931.8 and 951.8 eV, which corresponded to the typical values for Cu⁺ in Cu₂S.^{33,34} Meanwhile, there were no “shake-up” peaks in the higher binding energy direction, indicating the absence of CuS. In addition, the generation of Cu₂S could be demonstrated by the associated Auger line (Cu LMM) at 569.6 eV in Fig. 2b, which was the typical value of Cu₂S.³³ It was noted in Fig. 2 that the observed Cu 2p XPS and Auger Cu LMM peaks of Cu_xS/CdS were at the same positions with those for single Cu_xS, which revealed that copper in Cu_xS/CdS was also in the form of Cu⁺. On the basis of XRD and XPS results, we can summarize that Cu₂S and Cu_xS/CdS photocatalysts were finally synthesized in the present study.

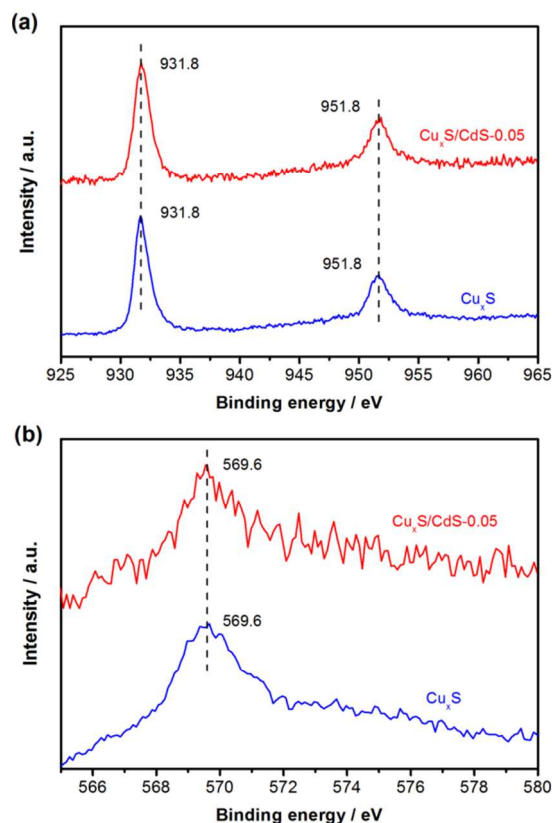
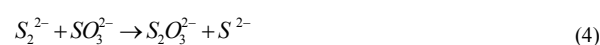


Fig. 2 (a) Cu 2p XPS spectra and (b) the Auger Cu LMM spectra of Cu_xS and Cu_xS/CdS-0.05 samples.

As presented in the experimental section, Cu₂S was obtained by adding 0.005 mol of Cu(NO₃)₂·3H₂O into 190 mL of 0.25 M Na₂SO₃/0.35 M Na₂S solution. In order to clarify the reaction process, 0.005 mol of Cu(NO₃)₂·3H₂O was respectively added into 190 mL of 0.25 M Na₂SO₃ or 0.35 M Na₂S solution for comparison. When Cu²⁺ was added into Na₂SO₃ solution and stirred for 0.5 h, the solution was still transparent and no solid products could be obtained. In the case of Cu²⁺ into Na₂S solution, black powders could be achieved, which could be denoted as Cu_xS (Na₂S). The XRD pattern of Cu_xS (Na₂S) showed the typical diffraction peaks assigned to both Cu₂S and CuS (Fig. S2). It is inferred that as Cu²⁺ was added into the solution with Na₂S, the equation (2) would occurred to form CuS due to its low solubility product (K_{sp}) of 6.3×10⁻³⁶.³⁵ Since the amount of S²⁻ (0.0665 mol) in the solution was much higher than the amount of added Cu²⁺ (0.005 mol), parts of CuS could be reduced to Cu₂S by excess S²⁻ according to the equation (3). Therefore, both Cu₂S and CuS were generated by adding Cu²⁺ into Na₂S solution. However, when Na₂SO₃ was present in the reaction solution, SO₃²⁻ would react with S₂²⁻ by the equation (4), accelerating the formation of Cu₂S by the equation (3). Meanwhile, CuS could be reduced to Cu₂S by SO₃²⁻ according to the equation (5). As a consequence, only Cu₂S was achieved by adding Cu²⁺ into the solution with both Na₂SO₃ and Na₂S.



3.2 Morphology and structure of Cu₂S/CdS hybrid photocatalysts

The morphology of Cu₂S/CdS hybrid photocatalysts was examined by FESEM. As shown in Fig. 3a and Fig. 3b, CdS nanocrystals exhibited polyhedral structure that had a size of several hundred nanometers. The surface of CdS polyhedrons is very clean and smooth. When Cu₂S were deposited to form Cu₂S/CdS, it was observed in Fig. 3c and Fig. 3d that a number of Cu₂S nanoparticles with a diameter of ca. 50 nm were adhered to the surface of CdS polyhedrons, and the heterojunctions between Cu₂S and CdS were acquired for Cu₂S/CdS-0.05. As the loading amount of Cu₂S was improved, more small nanoparticles deposited on CdS polyhedrons could be found for Cu₂S/CdS-0.1 in Fig. 3e and Fig. 3f. Particularly, the surfaces of CdS polyhedrons were nearly covered by the Cu₂S nanoparticles, and the polyhedral structure of CdS was hardly detected (Fig. 3e). Meanwhile, plenty of Cu₂S nanoparticles became to aggregate together (Fig. 3f).

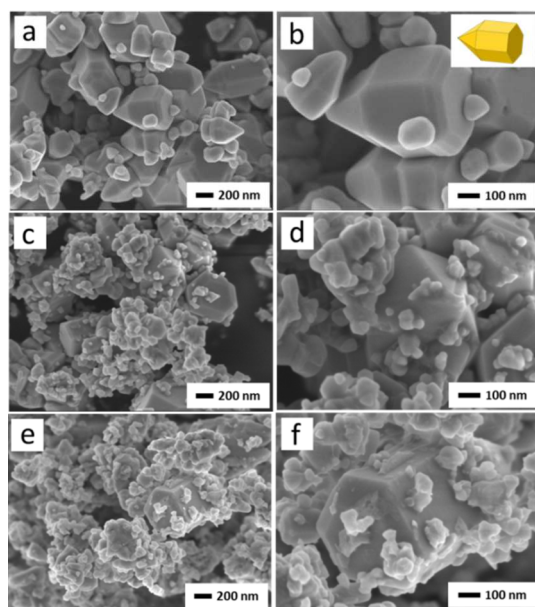


Fig. 3 FESEM images of (a, b) CdS; (c, d) Cu₂S/CdS-0.05; and (e, f) Cu₂S/CdS-0.1.

In order to further confirm the successful deposition of Cu₂S nanoparticles, EDX-SEM elemental mapping analysis of Cu₂S/CdS-0.05 was carried out. As displayed in Fig. 4, such mapping results demonstrated the presence of cadmium, copper and sulfur. In addition, it was observed in Fig. 4c that copper was uniformly dispersed, which indicated that well-dispersed heterojunctions between CdS and Cu₂S could be generated. The deposition process of Cu₂S nanoparticles could be illustrated in Fig. S3. CdS polyhedrons, serving as the substrates to deposit Cu₂S nanoparticles, were firstly dispersed into Na₂SO₃/Na₂S aqueous solution. Appropriate amount of aqueous solution containing Cu²⁺ ions was then dripped into the above suspension. Cu₂S would subsequently nucleate on the surface of polyhedral CdS nanocrystals and grew into crystallized nanoparticles. The Cu/Cd molar ratios of different Cu₂S/CdS photocatalysts were also determined by EDX system coupled with FESEM. As shown in Table S1, with the increase of added Cu precursor, the Cu/Cd

molar ratio by EDX gradually increased. Meanwhile, the measured Cu/Cd molar ratios are a little higher than the added ratios in the synthesis of Cu₂S/CdS samples, possibly due to Cu₂S nanoparticles deposited on the surface of polyhedral CdS nanocrystals (the analysis diameter and depth for the used EDX system is ca. 1.0 μm).

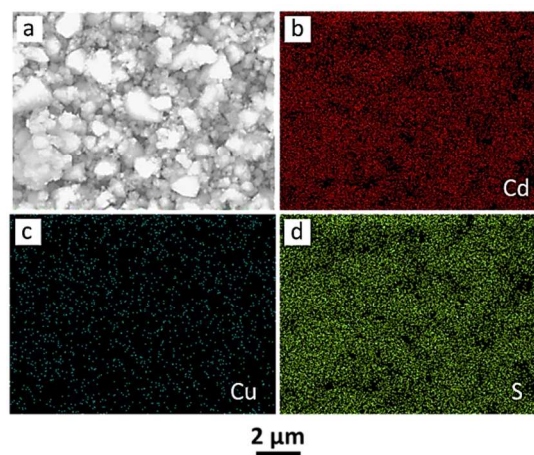


Fig. 4 (a) FESEM image of Cu₂S/CdS-0.05 and (b-d) the corresponding EDX-SEM mapping images of Cd, Cu and S in Cu₂S/CdS-0.05. The scale bar is 2 μm in each image.

TEM and HRTEM measurements were performed to identify the detailed structure of Cu₂S/CdS-0.05 hybrid photocatalysts. Fig. 5a shows a typical CdS polyhedron deposited by the highly dispersed Cu₂S nanoparticles with a diameter of ca. 50 nm (marked by red circles), which led to the formation of nanoscale heterojunctions between the CdS nanocrystal and Cu₂S nanoparticles. A close examination in Fig. 5b revealed that the contact between the two semiconductors was intimate, where the nanoscale heterojunction was at a lattice level. It was also discovered that the Cu₂S nanoparticle was completely crystalline. The clear lattice fringes with the interlayer spacing of 0.34 nm could be indexed to the (111) plane of cubic Cu₂S.^{31,32}

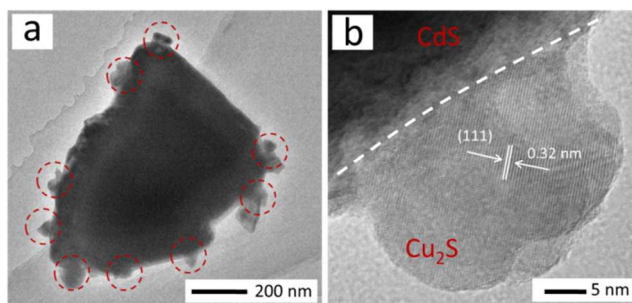


Fig. 5 (a) TEM image and (b) HRTEM image of Cu₂S/CdS-0.05.

3.3 Optical properties of Cu₂S/CdS hybrid photocatalysts

UV-vis absorption spectra of the prepared photocatalysts are shown in Fig. 6. The spectrum of pure CdS displayed sharp absorption edge at around 540 nm.³⁶ The absorption onsets of different Cu₂S/CdS photocatalysts were also located at around 540 nm, corresponding to the absorption of CdS in Cu₂S/CdS hybrid photocatalysts. The same absorption edges of pure CdS and Cu₂S/CdS indicated that copper was not doped into the bulk phase of CdS in Cu₂S/CdS hybrid photocatalysts. Compared to

the single CdS, Cu₂S/CdS showed an absorption band in the region of 550-750 nm, which should be ascribed to the contribution of Cu₂S, since its bandgap was reported to be 1.2 eV.²³ It was noted that the absorption intensity of this band gradually increased with the increasing amount of Cu₂S in Cu₂S/CdS.

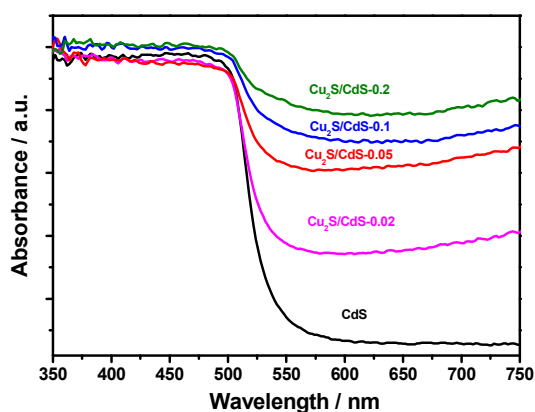


Fig. 6 UV-vis absorption spectra of Cu₂S/CdS hybrid photocatalysts with different Cu/Cd molar ratios.

Fig. 7 shows the room-temperature PL spectra of CdS and Cu₂S/CdS-0.05 under excitation at 420 nm. It was observed that the as-prepared CdS photocatalysts displayed a broad spectrum in the range of 500-850 nm with the main peak located at ca. 570 nm, which was close to the absorption onset of CdS (ca. 540 nm). The broad PL band generally revealed that a number of trapped states were formed in the forbidden band of CdS.³⁷ Wang et al. reported that the luminescence centered at 750 nm observed from the synthesized CdS nanowires should be trapped emission, which was mainly due to the surface defects (such as sulfur vacancies).³⁸ In our PL study, the emission between 650 and 850 nm was also considered to result from the surface defects of CdS. Such surface defects could act as the recombination centers of photoexcited charges to lower the photocatalytic efficiency for hydrogen production. As depicted in Fig. 7, the PL spectrum of Cu₂S/CdS-0.05 was similar to that of single CdS. However, the intensity was lower, verifying the higher charge separation efficiency in Cu₂S/CdS-0.05.³⁹ In particular, the emission intensity between 650 and 850 nm corresponding to the surface defect states of CdS was apparently decreased. It was reported by Kamat's group that Cu_xS could interact with defect states on the CdSe surface and quench emission resulting from selenide vacancies by forming p-n interfacial junction.⁴⁰ In the hybrid Cu₂S/CdS photocatalysts, similar mechanism can be expected. It was considered that Cu₂S could interact with the surface defects of CdS (such as sulfur vacancies), which could quench the emission between 650 and 850 nm from the surface trap states, leading to the much more efficient surface charge separation in Cu₂S/CdS hybrid photocatalysts.

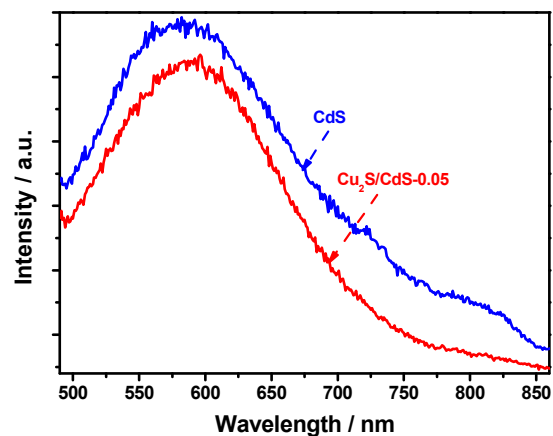


Fig. 7 PL spectra of CdS and Cu₂S/CdS-0.05. The excitation wavelength was 420 nm.

3.4 Photocatalytic hydrogen production

Photocatalytic performances of as-prepared samples for hydrogen production are displayed in Fig. 8a. The photocatalytic activity of single CdS was 50.1 $\mu\text{mol h}^{-1}$. Cu₂S deposition could improve the photocatalytic hydrogen production efficiently. When the loading amount of Cu₂S was gradually increased, the photocatalytic activity was firstly increased and then decreased. With the optimal Cu/Cd molar ratio of 0.05, the hydrogen production rate of Cu₂S/CdS was 400.1 $\mu\text{mol h}^{-1}$, which was nearly 8 times higher than that of single CdS. The apparent quantum yield of Cu₂S/CdS-0.05 at 420 nm was calculated to be 9.5%. When the Cu/Cd molar ratio was below 0.05, the increased Cu₂S amount could lead to higher photocatalytic hydrogen production. However, as the Cu/Cd molar ratio exceeded 0.05, the surface of CdS polyhedrons was nearly covered by Cu₂S nanoparticles (Fig. 3e and Fig. 3f), which may affect the efficient utilization of light by CdS photocatalysts. Meanwhile, more Cu₂S nanoparticles tended to aggregate together (Fig. 3e and Fig. 3f), which could lead to the increased recombination of photoexcited charges at Cu₂S nanoparticles. Therefore, the photocatalytic activity was gradually decreased when excess Cu₂S was deposited. The photocatalytic performance of pure Cu₂S was also studied. However, no hydrogen could be detected, possibly resulting from the low charge separation efficiency in Cu₂S nanoparticles.⁴¹ Long-time photocatalytic test of Cu₂S/CdS-0.05 sample for hydrogen production was carried out to evaluate the stability of Cu₂S/CdS hybrid photocatalysts. As shown in Fig. 8b, there was no apparent decrease in the photocatalytic activity over the 20 hours' reaction, indicating the good stability of Cu₂S/CdS-0.05. In order to further investigate the stability of Cu₂S on the surface of CdS, we carried out the XPS measurement to study the valence state of Cu₂S/CdS-0.05 sample after long-time photocatalytic reaction. It was noted in Fig. S4 that the observed Cu 2p peaks of Cu₂S/CdS-0.05 sample before and after long-time photocatalytic reaction were at the same positions, revealing the good stability of Cu₂S in Cu₂S/CdS during the photocatalytic reaction.

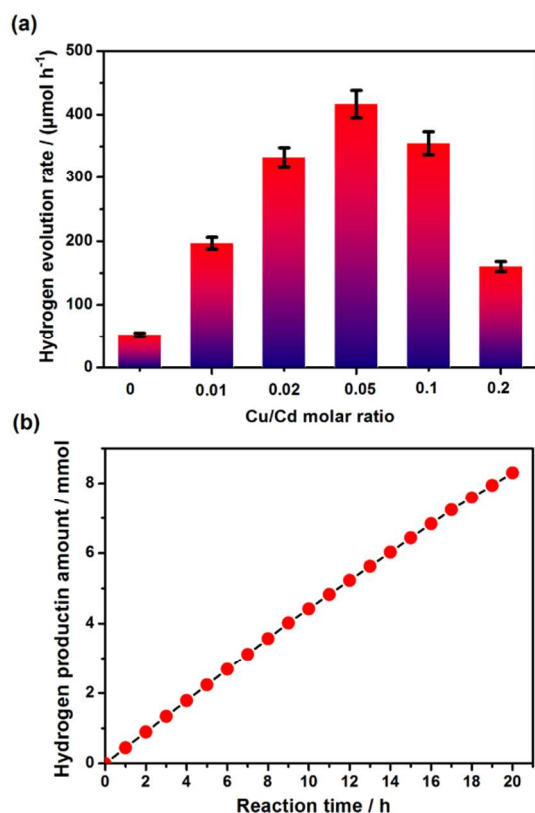


Fig. 8 (a) Photocatalytic hydrogen production over Cu₂S/CdS hybrid photocatalysts with different Cu/Cd molar ratios and (b) long-time photocatalytic test of Cu₂S/CdS-0.05 sample for hydrogen production. Reaction conditions: 0.2 g of CdS photocatalyst; appropriate amount of Cu₂S deposited by the in-situ method; 190 mL of aqueous solution containing 0.25 M Na₂SO₃/0.35 M Na₂S; 300 W Xe lamp equipped with a cutoff filter ($\lambda \geq 420$ nm).

As analysed from the PL results of CdS and Cu₂S/CdS photocatalysts (Fig. 7), Cu₂S deposition could lead to the more efficient charge separation in CdS, which was considered to be the key factor for the improved activity of Cu₂S/CdS. The schematic diagram of the charge separation process in Cu₂S/CdS could be illustrated in Fig. 9. As mentioned above, CdS and Cu₂S are respectively n-type and p-type semiconductors. Meanwhile, as shown in Fig. S5, a negative slope of the linear region in the Mott-Schottky plot of Cu₂S film indicated the p-type semiconductor character of Cu₂S.²⁷ When n-type CdS polyhedrons were coupled with p-type Cu₂S nanoparticles, large amounts of nanoscale p-n junctions could be generated between the two semiconductors (Fig. 5). Across the p-n junction a built-in electric field is formed, where the p-type Cu₂S region is negatively charged (Fig. 9a), and the n-type CdS region is positively charged (Fig. 9a). Considering the band structures of Cu₂S and CdS, it has been reported that both the conduction band (CB) and the valence band (VB) of Cu₂S are higher than those of CdS.^{25,42} When Cu₂S and CdS formed p-n heterojunction, the electron transfer occurred from Cu₂S to CdS while the hole transfer occurred from CdS to Cu₂S due to the different Fermi levels until the system attained equilibration. The proposed band profile for Cu₂S/CdS heterojunction was shown in Fig. 9b.^{24,43}

When Cu₂S/CdS hybrid photocatalysts were irradiated with visible light, the photoexcited electrons and holes would be both

obtained in CdS and Cu₂S. As a result of the built-in electric field, the photogenerated electrons in the CB of Cu₂S would diffuse into the CB of CdS through the p-n junction, giving rise to the accumulation of photogenerated electrons in the CdS nanocrystal. Likewise, the photogenerated holes in the VB of CdS would diffuse into the VB of Cu₂S, leading to the accumulation of photogenerated holes in the Cu₂S nanoparticle. As a consequence, the efficient charge separation was successfully achieved by the nanoscale p-n junctions in Cu₂S/CdS. Meanwhile, the close interaction between CdS and Cu₂S (Fig. 5b) could facilitate the charge transfer.⁴⁴ Subsequently, the accumulated electrons would transfer to the surface of CdS to reduce H⁺ for hydrogen production, and the accumulated holes would transfer to the surface of Cu₂S to oxidize the sacrificial reagents (S²⁻, SO₃²⁻). The improved photocatalytic activity was acquired through the efficient charge separation. During the photocatalytic reaction, Cu₂S nanoparticles captured the photogenerated holes in CdS and functioned as the active sites for the surface oxidation reaction.

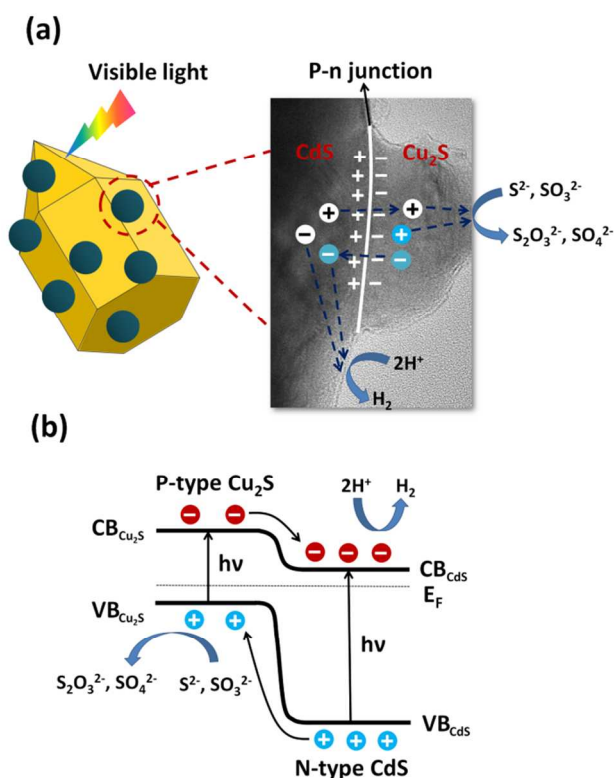


Fig. 9 (a) The schematic diagram of forming p-n junction and charge transfer process in Cu₂S/CdS and (b) the band structure for Cu₂S/CdS heterojunction and charge separation process under illumination.

Although the charge separation could be achieved for Cu₂S/CdS with different Cu/Cd molar ratios through the nanoscale p-n junctions, the efficiency of charge separation was not the same. As the Cu/Cd molar ratio is below 0.05, Cu₂S nanoparticles were uniformly dispersed on the surface of CdS polyhedron. More nanoscale p-n junctions could be generated with the increased Cu₂S nanoparticles deposited, resulting in higher charge separation efficiency and better photocatalytic performance. However, when the Cu/Cd molar ratio was above 0.05, the aggregation of Cu₂S nanoparticles occurred, which

restricted the formation of more p-n junctions. Meanwhile, the grain boundaries of Cu₂S nanoparticles would act as the recombination centers, leading to lower charge separation efficiency.⁴⁵ Further increasing the amount of Cu₂S would give rise to the decreased photocatalytic activity.

Single Cu₂S could not produce hydrogen possibly owing to its low charge separation efficiency. However, in Cu₂S/CdS hybrid photocatalysts, the efficient charge separation from nanoscale p-n junctions was achieved, which could promote the utilization of photoexcited charges in Cu₂S for photocatalytic reaction. This result implied that more visible light could be harvested by Cu₂S/CdS for photocatalytic hydrogen production compared to single CdS, which should also contribute to the enhanced activity.

Table 1. Photocatalytic hydrogen production of different photocatalysts with and without Cu₂S.

| Sample | Hydrogen production rate without Cu ₂ S | Hydrogen production rate with Cu ₂ S |
|----------------------------------|--|---|
| ZnIn ₂ S ₄ | 5.0 μmol h ⁻¹ | 30.9 μmol h ⁻¹ |
| TiO ₂ | 0.5 μmol h ⁻¹ | 16.0 μmol h ⁻¹ |

In order to demonstrate whether p-type Cu₂S can enhance the activities of other n-type semiconductor photocatalysts. Cu₂S was respectively coupled with n-type ZnIn₂S₄ and n-type TiO₂ to generate Cu₂S/ZnIn₂S₄ and Cu₂S/TiO₂ hybrid photocatalysts with p-n junction heterostructures. The photocatalytic hydrogen production of different photocatalysts with and without Cu₂S were tested. The detailed synthesis and photocatalytic process of Cu₂S/ZnIn₂S₄ and Cu₂S/TiO₂ photocatalysts can be found in the supporting information. As shown in Table 1, the hydrogen production rates of single ZnIn₂S₄ and TiO₂ were rather low. After loading Cu₂S, both photocatalytic activities were apparently improved. This result indicated that Cu₂S was suitable for various photocatalysts. No matter the photocatalyst is either metal sulfide or metal oxide, Cu₂S could efficiently promote the photocatalytic hydrogen production. The nanoscale p-n junctions between p-type Cu₂S and n-type semiconductor, leading to more efficient charge separation, are considered to be the key factor for the improved activities. The present study thus provides a general strategy to develop efficient Cu₂S-modified photocatalysts by forming p-n junction structure.

4. Conclusions

In summary, Cu₂S/CdS heterostructure was successfully synthesized by the in-situ deposition of Cu₂S onto CdS photocatalysts. Cu₂S nanoparticles were tightly attached on the surface of polyhedral CdS nanocrystals in Cu₂S/CdS, which led to the formation of nanoscale p-n junctions between p-type Cu₂S nanoparticles and n-type CdS polyhedrons. Cu₂S deposition could apparently improve the photocatalytic hydrogen production of CdS photocatalysts. The generated nanoscale p-n junctions in Cu₂S/CdS, leading to the enhanced charge separation efficiency and better utilization of visible light, were considered to be the key factor for the significantly enhanced property. The photocatalytic hydrogen production of Cu₂S/CdS photocatalysts was related with the Cu/Cd molar ratio. With the optimal Cu/Cd molar ratio of 0.05, the apparent quantum yield of Cu₂S/CdS at

420 nm reached 9.5%. P-type Cu₂S could also improve the photocatalytic activities of n-type ZnIn₂S₄ and n-type TiO₂ by forming efficient p-n junction structure, indicating the general applicability of p-type Cu₂S. This work not only demonstrates that low-price and environment-friendly p-type Cu₂S could promote the photocatalytic activities of various n-type semiconductor photocatalysts but also proposes an effective guidance to developing efficient noble-metal-free hybrid photocatalysts by forming p-n junction structure.

Acknowledgments

The authors thank the financial support from the National Natural Science Foundation of China (Nos. 51323011 and 51236007) and the grant support from the China Postdoctoral Science Foundation (No. 2014M560768).

*Corresponding author: Dr. Y. Chen and Prof. L. Guo. International Research Center for Renewable Energy, State Key Laboratory of Multiphase Flow in Power Engineering, Xi'an Jiaotong University, Shaanxi 710049, P. R. China.
E-mail: ybchen@mail.xjtu.edu.cn; lj-guo@mail.xjtu.edu.cn.

† Electronic Supplementary Information (ESI) available: The detailed synthesis and photocatalytic process of Cu₂S/ZnIn₂S₄ and Cu₂S/TiO₂ photocatalysts; The calculation method of the number of incident photons; The Cu/Cd molar ratios determined by EDX of different Cu₂S/CdS samples; The schematic diagram of the photocatalytic reactor for hydrogen production; XRD patterns of Cu_xS (Na₂S) sample and Cu₂S (Na₂SO₃/Na₂S) sample (Cu₂S achieved by adding Cu²⁺ into Na₂SO₃/Na₂S solution); Illustration of the deposition process of Cu₂S nanoparticles on CdS polyhedrons; Cu 2p XPS spectra of Cu₂S/CdS-0.05 sample before and after long-time photocatalytic reaction; Mott-Schottky plot of Cu₂S film. See DOI: 10.1039/b000000x/

References

- X. Chen, S. Shen, L. Guo and S. Mao, *Chem. Rev.*, 2010, **110**, 6503.
- K. Shimura and H. Yoshida, *Energy Environ. Sci.*, 2011, **4**, 2467.
- K. Maeda and K. Domen, *J. Phys. Chem. Lett.*, 2010, **1**, 2655.
- J. Yang, D. Wang, H. Han and C. Li, *Acc. Chem. Res.*, 2013, **46**, 1900.
- Y. H. Li, J. Xing, Z. J. Chen, Z. Li, F. Tian, L. R. Zheng, H. F. Wang, P. Hu, H. J. Zhao and H. G. Yang, *Nat. Commun.*, 2013, **4**, 2500.
- C. Kong, S. Min and G. Lu, *Chem. Commun.*, 2014, **50**, 9281.
- Z. Xiong, H. Yan, G. Wu, G. Ma, F. Wen, L. Wang and C. Li, *J. Am. Chem. Soc.*, 2008, **130**, 7176.
- X. Zong, J. Han, G. Ma, H. Yan, G. Wu and C. Li, *J. Phys. Chem. C*, 2011, **115**, 12202.
- W. Zhang, Y. Wang, Z. Wang, Z. Zhong and R. Xu, *Chem. Commun.*, 2010, **46**, 7631.
- L. Zhang, T. Xie, D. Wang, S. Li, L. Wang, L. Chen and Y. Lu, *Int. J. Hydrogen Energy*, 2013, **38**, 11811.
- L. Ma, F. Li, Z. Sun, M. Liu, Y. Wang and L. Xu, *RSC Adv.*, 2014, **4**, 21369.
- M. Tabata, K. Maeda, T. Ishihara, T. Minegishi, T. Takata and K. Domen, *J. Phys. Chem. C*, 2010, **114**, 11215.
- L. Zhang, B. Tian, F. Chen and J. Zhang, *Int. J. Hydrogen Energy*, 2012, **37**, 17060.
- P. Gomathisankar, K. Hachisuka, H. Katsumata, T. Suzuki, K. Funasaka and S. Kaneco, *Int. J. Hydrogen Energy*, 2013, **38**, 8625.
- J. Xu, Y. Li and S. Peng, *Int. J. Hydrogen Energy*, 2015, **40**, 353.
- Y. Chen and L. Guo, *J. Mater. Chem.*, 2012, **22**, 7507.
- F. Meng, J. Li, S. K. Cushing, M. Zhi and N. Wu, *J. Am. Chem. Soc.*, 2013, **135**, 10286.
- A. J. Frank and K. Honda, *J. Phys. Chem.*, 1982, **86**, 1933.
- A. Serpi, *J. Phys. D: Appl. Phys.*, 1976, **9**, 1881.

- 20 B. C. O'Regan and F. Lenzmann, *J. Phys. Chem. B*, 2004, **108**, 4342.
- 21 J. Lin, J. Shen, R. Wang, J. Cui, W. Zhou, P. Hu, D. Liu, H. Liu, J. Wang, R. I. Boughton and Y. Yue, *J. Mater. Chem.*, 2011, **21**, 5106.
- 22 J. Zhang, S. Z. Qiao, L. Qi and J. Yu, *Phys. Chem. Chem. Phys.*, 2013, **15**, 12088.
- 23 Z. Zhuang, Q. Peng, B. Zhang and Y. Li, *J. Am. Chem. Soc.*, 2008, **130**, 10482.
- 24 W. D. Gill and R. H. Bube, *J. Appl. Phys.*, 1970, **41**, 3731.
- 25 Y. Wu, C. Wadia, W. Ma, B. Sadtler and A. P. Alivisatos, *Nano Lett.*, 2008, **8**, 2551.
- 26 C. Pan, S. Niu, Y. Ding, L. Dong, R. Yu, Y. Liu, G. Zhu and Z. L. Wang, *Nano Lett.*, 2012, **12**, 3302.
- 27 Y. Bessekhouad, R. Brahim, F. Hamdini and M. Trari, *J. Photochem. Photobiol. A: Chem.*, 2012, **248**, 15.
- 28 Y. Zhao and C. Burda, *Energy Environ. Sci.*, 2012, **5**, 5564.
- 29 Y. Liang, M. Shao, L. Liu, J. G. McEvoy, J. Hu and W. Cui, *Catal. Commun.*, 2014, **46**, 128.
- 30 Y. Li, Y. Hu, S. Peng, G. Lu and S. Li, *J. Phys. Chem. C*, 2009, **113**, 9352.
- 31 Z. Li, H. Yang, Y. Ding, Y. Xiong and Y. Xie, *Dalton Trans.*, 2006, 149.
- 32 J. Liu and D. Xue, *Adv. Mater.*, 2008, **20**, 2622.
- 33 M. Yan, C. Chen, N. Zhang, X. Wen, W. Guo and C. Lin, *Adv. Energy Mater.*, 2014, **4**, 1301564.
- 34 Y. Liu, Y. Deng, Z. Sun, J. Wei, G. Zheng, A. M. Asiri, S. B. Khan, M. M. Rahman and D. Zhao, *Small*, 2013, **9**, 2702.
- 35 J. Zhang, J. Yu, Y. Zhang, Q. Li and J. R. Gong, *Nano Lett.*, 2011, **11**, 4774.
- 36 D. Jing and L. Guo, *J. Phys. Chem. B*, 2006, **110**, 11139.
- 37 Y. Lin, J. Zhang, E. H. Sargent and E. Kumacheva, *Appl. Phys. Lett.*, 2002, **81**, 3134.
- 38 Y. Wang, G. Meng, L. Zhang, C. Liang and J. Zhang, *Chem. Mater.*, 2002, **14**, 1773.
- 39 J. Hou, C. Yang, Z. Wang, S. Jiao and H. Zhu, *RSC Adv.*, 2012, **2**, 10330.
- 40 J. G. Radich, N. R. Peeples, P. K. Santra and P. V. Kamat, *J. Phys. Chem. C*, 2014, **118**, 16463.
- 41 B. Wang, W. An, L. Liu, W. Chen, Y. Liang and W. Cui, *RSC Adv.*, 2015, **5**, 3224.
- 42 X. Li, H. Shen, S. Li, J. Z. Niu, H. Wang and L. S. Li, *J. Mater. Chem.*, 2010, **20**, 923.
- 43 G. L. Lazarev, *J. Appl. Phys.*, 1980, **51**, 4257.
- 44 X. Wang, G. Liu, Z. G. Chen, F. Li, L. Wang, G. Q. Lu and H. M. Cheng, *Chem. Commun.*, 2009, **23**, 3452.
- 45 S. C. Riha, R. D. Schaller, D. J. Gosztola, G. P. Wiederrecht and A. B. F. Martinson, *J. Phys. Chem. Lett.*, 2014, **5**, 4055.